Design and Optimization of a Ring-Pair Permanent Magnet Array for Head Imaging in a Low-Field Portable MRI System

Zhi Hua Ren, Wen Chuan Mu, and Shao Ying Huang

Division of Engineering Product Development, Singapore University of Technology and Design, Singapore 487372

In this paper, we present the design and optimization of a ring-pair permanent magnet array for head imaging in a low-field portable magnetic resonance imaging (MRI) system. The proposed array generates a longitudinal main static magnetic field (B_0 field) with an average field strength of 169.7 mT and a homogeneity of 24786 ppm in a field of view with a diameter of 200 mm and a thickness of 50 mm. It is a significant increase in field homogeneity by 79.7% compared to a traditional ring-pair structure of the same dimension and mass while still maintaining a similar field strength. The optimization was implemented by applying a genetic algorithm and by proposing an efficient current model for the forward calculation of the magnetic field. The effectiveness of the optimization is validated by realistic simulations using COMSOL Multiphysics. Compared to a Halbach array, where the field is transversal and the existing coil designs cannot be applied directly, the proposed array generates stronger fields. Its magnetic field is longitudinal, which allows the direct application of the advancements in RF coil designs in a conventional MRI system to the imaging system using the proposed magnet array.

Index Terms— **Current density model, genetic algorithm (GA), homogeneous magnetic field, low-field magnetic resonance imaging (MRI), magnet array, permanent magnet, portable MRI.**

I. Introduction

THE majority of clinical magnetic resonance imaging (MRI) scanners are based on the superconducting magnet. They are bulky, heavy, and costly to purchase, site, and maintain. The disadvantages of a conventional MRI system have led to increasing interests in the development of a portable MRI scanner [1]–[4]. Portable MRI scanners may provide a supplementary medical imaging solution to a moving environment (e.g., the ambulance and the field hospital), to rural areas, or to underdeveloped areas/countries due to their low cost, portability, and compatibility with patients having metallic implants compared with the conventional MRI scanners based on superconducting magnets. To make an MRI scanner portable, it is inevitable to replace the superconducting magnet that takes up a large percentage of the space of the system with other mechanisms to supply the $\boldsymbol{B}_0$ field. Moreover, building the apparatus around the part of the human body under imaging rather than a whole body coverage helps to achieve the compactness of the system. Being supported by these two thoughts, portable MRI imaging systems have been proposed by building a magnet or a magnet array and radio frequency (RF) coils around the object under scanning (e.g., head and extremities) [2]–[4]. The magnet array in such a system is kept to be compact to make the system compact. In this approach, electromagnets and permanent magnet arrays are good options to provide the $\boldsymbol{B_0}$ field. However, it is challenging because such a magnet system is required to have high field strength and high field homogeneity within a field of view (FOV) that can accommodate the parts of human body (for example, human head). A high field strength leads to high signal-to-noise ratio and thus a high spatial resolution for imaging, whereas a high homogeneity leads to a small working bandwidth and thus a possible high-quality factor (Q-factor) for the RF coils and spectrometer console. Moreover, a high homogeneity is necessary for the use of traditional gradient coils and the application of many traditional MRI sequences.

For electromagnets, they generate static magnetic fields using dc currents. They could be installed relatively easily and can be switched off anytime. However, electromagnets are limited by a small output magnetic field and a large size. Electromagnets dissipate a considerable amount of heat, which limits the input power and consequently caps the field strength they can generate. Moreover, the size of such an electromagnet has to be much larger than an FOV. In 2015, Sarracanie *et al.* [3] introduced a low-cost MRI system using an electromagnet. This custom built biplanar electromagnet [5] has a cross-sectional outer diameter of 220 cm, a width of 90 cm, and a weight of about 340 kg for generating an average field strength of 6.5 mT and a homogeneity of about 100 ppm within an FOV with a diameter of 40 cm (head sized) [6].

A permanent magnet system is a popular option to generate $\boldsymbol{B_0}$ field with a compact size, no electric power consumption, no heat dissipation thus no cryogen system needed, and relatively low cost. Mainly, there are two types of systems that have been used for portable MRI systems. One is a magnetic circuit consisting of two poles (with aggregated magnets) and an iron yoke. In such a system, the space between the two poles is used for imaging. The H-shaped and the C-shaped magnet yoke in Fig. 1(a) and (b), respectively, are the two examples of such a system. The poles consist of small magnet blocks stacked up. The disadvantages of such a system are that the size and weight of the system are proportional to the FOV. The iron yoke could guide and concentrate the magnetic

Manuscript received April 3, 2018; revised August 21, 2018; accepted October 5, 2018. Date of publication November 12, 2018; date of current version December 18, 2018. Corresponding author: S. Y. Huang (e-mail: huangshaoying@sutd.edu.sg).

Color versions of one or more of the figures in this paper are available online at http://ieeexplore.ieee.org.

Digital Object Identifier 10.1109/TMAG.2018.2876679

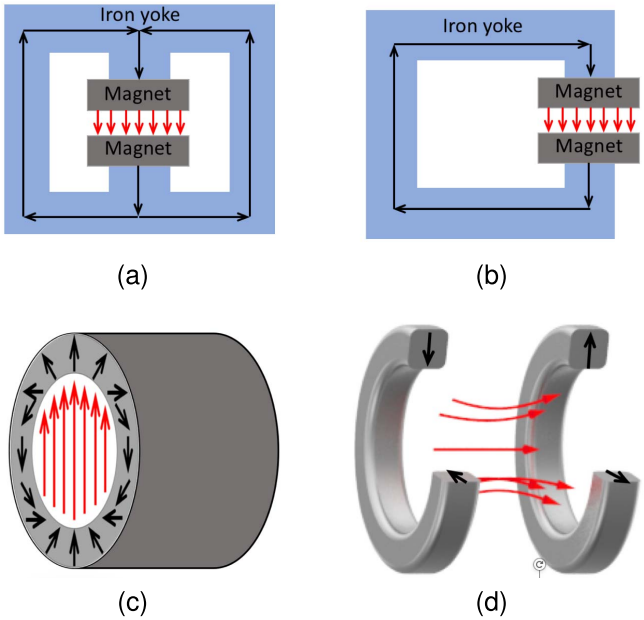

Fig. 1. Illustration of (a) H-shaped magnet, (b) C-shaped magnet, (c) Halbach cylinder [9], and (d) sectional view of an Aubert ring pair [10].

flux, thus greatly reduce the fringe field. However, it increases the weight and size of the magnet assembly dramatically [7]. Usually, the FOV is much smaller than the size of the magnetic poles. For an FOV of a head size, the system can take up to a room size ($>$ 30 m^2) and a weight over 10 t [8]. Kimura *et al.* [1] developed a mobile MRI system for imaging the outdoor trees based on a C-shaped magnet. The magnet assembly has a total weight of 57 kg with a gap of 80 mm. It generates a $\boldsymbol{B_0}$ field with an average field strength of 0.3 T and the field homogeneity of 60 ppm in a spherical volume with a diameter of 30 mm.

The other type of permanent magnet system is the permanent magnet array. Halbach array proposed by Halbach [9], and the yokeless magnet ring pair proposed by Aubert (named Aubert ring pair in this content) [10], are the two representatives of this category. These are shown in Fig. 1(c) and (d), respectively. An ideal Halbach cylinder is an infinitely long cylindrical magnet with a continuously varying polarization in the azimuthal direction. The polarizations are indicated by the black arrows in Fig. 1(c). It generates a single directional homogeneous transverse field inside the bore of the magnet cylinder (indicated by the red color arrows), and negligible fringe fields outside. A Halbach array is an implementation of a Halbach cylinder where the cylinder is discretized in the azimuthal direction and built by using permanent magnet bars, cubes, and cylinders. The discretization makes a Halbach array relatively lightweight compared to other permanent magnet systems. However, on the other hand, the field strength and homogeneity are lowered by the sparse discretization. Shimming using small magnet cubes was proposed to compensate for the degradation caused by the discretization [2], [11]. In recent years, Halbach array has been used to provide the $\boldsymbol{B}_0$ field in a portable MRI system [2], [4], [11]–[13]. Cooley *et al.* [12] reported the design and optimization of a sparse Halbach cylinder using genetic algorithm (GA) and finite-element simulations. In this paper, by using GA, the field inhomogeneity was significantly reduced by 95%. In a Halbach array, due to the transversal direction of the $\boldsymbol{B}_0$ field, the existing design of RF coils for conventional MRI scanners has to be re-engineered for the system using a Halbach array.

Aubert ring pair as shown in Fig. 1(d) consists of two magnet rings with opposite radial polarization (illustrated by black arrows), one inward and the other outward. The combination of the two rings generates a confined longitudinal field (illustrated by red arrows) in the central volume of the structure. When it is applied for MRI imaging, due to the fact that the direction of the magnetic field is the same as that in a superconducting-magnet-based MRI system, the existing designs and advancement of RF coils for conventional MRI scanners can be applied directly. For this reason, Aubert ring pair has started to capture attention for its application in a low-field portable MRI system [14], [15]. However, with the current design, the homogeneities and field strength of the magnetic field are not enough for MRI imaging in a head-size FOV. In [14], the development of an Aubert ring pair was reported. The ring pair consists of 48 identical NdFeB magnet cubes with a dimension of 12 $\times$ 12 $\times$ 12 mm. It produces a magnetic field with an average field strength of 100 mT and a field homogeneity of 40 ppm in a volume of 5 mm^3. The magnet assembly has a bore of 52 mm diameter. Further optimization on an Aubert ring pair is needed before it can be used in a portable MRI system for imaging.

In this paper, the design and optimization of a ring-pair permanent magnet array are reported for head imaging in a portable MRI system. The design is based on the Aubert ring pair. In the proposed design process, GA was applied for the optimization of field strength and homogeneity in a cylindrical FOV of 200 mm in diameter and 50 mm in length at the center of the magnet bore. In the optimization loop, a simplified current model was proposed to accelerate the calculation of the magnetic field with accuracy. In Section II, the design and optimization including the application of GA and the proposed simplified current model is detailed. In Section III, simulated results of the optimized magnet array are presented which shows a significant improvement in the field homogeneity after the optimization compared to an Aubert ring pair with a similar dimension and the same mass of magnetic material before the optimization. Discussion on the design and optimization is presented in Section IV and a conclusion is made in Section V.

II. Design and Optimization

The proposed ring-pair permanent magnet array is an aggregate of Aubert ring pairs [shown in Fig. 1(d)]. It is an assembly of these Aubert ring pairs with the axis of the rings aligned with the z-axis, as shown in Fig. 2. Fig. 2(a) and (b) shows the 3-D view and 2-D side view of the proposed design, respectively. An Aubert ring pair is indicated in blue in both Fig. 2(a) and (b). In the proposed design, as shown in Fig. 2(b), each ring pair has an inner radius of R^i_{in}, an outer radius of R^i_{out}, a thickness of t_i, z^{ij}_1, and z^{ij}_2, respectively, are the

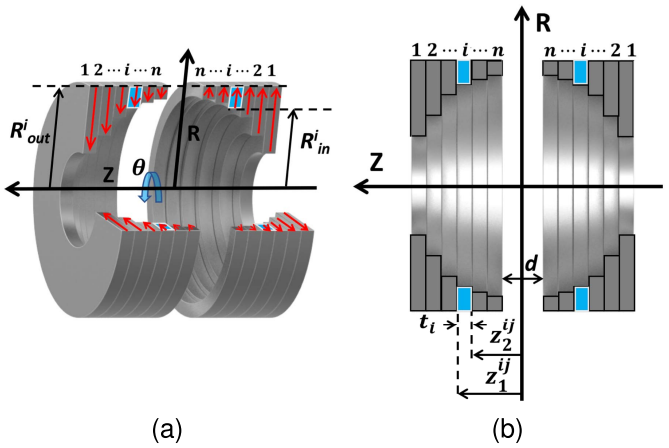

Fig. 2. Proposed ring-pair permanent magnet array. (a) 3-D view where the polarization of each ring is indicated by the red arrows and R^i_{in}ï¼Œ R^i_{out} are labeled. (b) Side view where z_1^{ij}, z_2^{ij}, t_i, and d are labeled.

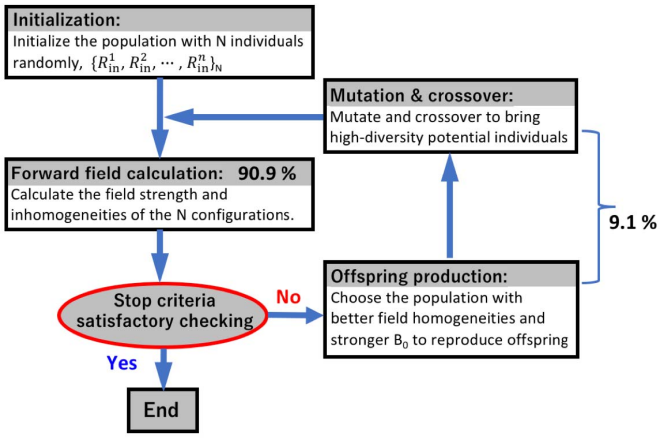

Fig. 3. Flowchart of the GA.

coordinates of the outer surface and the inner surface of the i_{th} magnet ring along the z-axis defining the location of the ring along the z-axis, $j = 1, 2$ indicating the left and right rings, respectively. A distance between the two inner surfaces of the two innermost rings is defined as d, and i is the index of the ring pair when the ring pairs are indexed outside in. In the design, the dimensions of the proposed magnet array, R^i_{in}, R^i_{out}, and t_i, and the number of ring pairs could be optimized toward achieving a high field homogeneity and a high field strength. For head imaging in 2-D, the FOV is set to be a cylindrical volume with a diameter of 200 mm and a length of 50 mm at the center of the magnet bore. For the optimization, GA was applied and an efficient current model was proposed and used for a fast forward calculation. The details are presented next.

A. Genetic Algorithm

GA is a random search algorithm based on the natural selection theory of biological evolution. It provides potential solutions with high diversity [16], [17]. Generally, the GA contains improvement iterations where offspring are produced, crossovered, and mutated. GA has shown its effectiveness for this kind of nonlinear optimization of magnet design for MRI systems [12], [18], [19]. In this paper, the optimization objectives are high field strength (>160 mT) and high field homogeneity (<20 000 ppm) within a cylindrical FOV (diameter = 200 mm and length = 50 mm) at the center of the magnet bore for head imaging.

To facilitate the implementation, R^i_{out} for each layer is set to be 250 mm. The total number of layers for each side is set to be 10, and the thicknesses for each layer are set to be 10 mm. All the magnets are set to be magnetized with a remanence of 1.4 T. Fig. 3 shows the flow of applying GA for the design of the ring-pair permanent magnet array. The first step is to initialize the population with N individuals randomly. There are 11 parameters in one individual, R^i_{in} $(i = 1, 2, \ldots, 10)$ and the distance d between the two innermost rings. The population size is set to be 100 to provide enough diversity for the solution. Following the initialization, the magnetic field is calculated for the N configurations of the parameters in the N individuals in the preset FOV. Fitness values are calculated based on the calculated fields. They are examined based on the stopping criteria which are the field strength and field homogeneity in the FOV. If the stopping criteria are not satisfied, the populations with high field strength and field homogeneity are chosen to produce offspring based on the calculated fitness values. Afterward, mutations and crossovers are applied to the produced offspring to bring diversity to the population. Then, the magnetic field and the fitness values are calculated again for the N configurations in the population. Another iteration is initiated again when the criteria are not satisfied whereas the optimization is ended when the criteria are met.

In the flow in Fig. 3, the time it takes for each step in terms of the percentage of the total optimization time is labeled. As can be seen, the optimization only takes less than 10%, however, the forward calculation of magnetic fields of the magnet array under optimization consumes more than 90% of the time when COMSOL Multiphysics was used. The speed of the forward calculation decides the speed of optimization. A fast calculation with accuracy is crucial for an optimization that can be done within a practical amount of time. A current model for the calculation of magnetic field offers both high calculation speed and high accuracy. In this paper, it was simplified and accelerated for the field calculation for the optimization. The derivation and validation are presented in Section II-B.

B. Simplified Current Model for an Accelerated Forward Field Calculation

A fast calculation of the field strength is crucial for the acceleration of the optimization. In the literature, there are different calculation methods for a magnet system. For a system with both magnets and iron, such as a C-shaped system and an H-shaped system, numerical methods such as boundary integral method [20], [21] and finite-element method (FEM) [12], [22] can handle the calculations of the magnetic fields. The forward model can be accelerated for

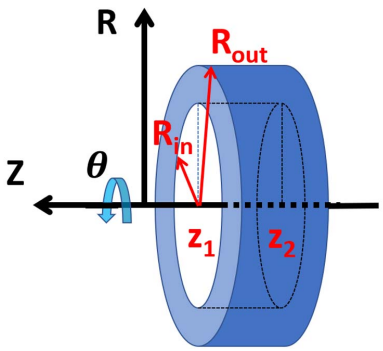

Fig. 4. Magnet ring with the axis aligned with the z-axis in a cylindrical coordinate system. The magnet ring is radially polarized outward.

an optimization. One example is Cooley *et al.* [12] used finite-element simulations for the forward calculation of magnetic fields. The calculation was simplified by fixing the overall magnet size and extent before the optimization of the combination of the material choice (no magnet or N42 or N52 grade material) allocated for each space. For a system with magnets only, such as a Halbach array, an Aubert ring pair, and the proposed ring-pair permanent magnet array in this paper, physical models such as the current model (or named current density model) [23] that are much simpler compared to numerical methods. A physical model could offer calculation efficiency due to simplicity. For the proposed ring-pair magnet array, since it only consists of magnets and is axially symmetric, the current model was chosen and was simplified for a fast forward calculation for the optimization.

For the magnetic field generated by permanent magnets, the principle of superposition holds. Therefore, the calculation of the total magnetic fields generated by the proposed ring-pair magnet array can be done by summing up the fields generated by each ring. Fig. 4 shows a single ring of the proposed array. The application and simplification of the current model for the calculation of the magnetic field generated by such a ring is detailed next.

In the current model, a permanent magnet is reduced to the distribution of equivalent currents. For a permanent magnet ring shown in Fig. 4, there are only equivalent surface currents. The magnetic field generated by these equivalent currents can be calculated by as follows [23]:

$$\boldsymbol{B}(\boldsymbol{r}) = \frac{\mu_0}{4\pi} \oint_S \boldsymbol{j_m}(\boldsymbol{r}') \times \frac{\boldsymbol{r} - \boldsymbol{r}'}{|\boldsymbol{r} - \boldsymbol{r}'|^3} ds' \tag{1}$$

where $\boldsymbol{r} = \langle r, \theta, z \rangle$ is the observation point, $\boldsymbol{r}' = \langle r', \theta', z' \rangle$ is the point of current source, and S is the surface of the magnet. Cylindrical coordinate system is used. For a single magnet ring with an outward radial polarization, the equivalent surface current source is expressed as follows:

$$\boldsymbol{j_m} = \begin{cases} -M_0 \hat{\theta}', & z = z_1 \\ M_0 \hat{\theta}', & z = z_2 \end{cases} \tag{2}$$

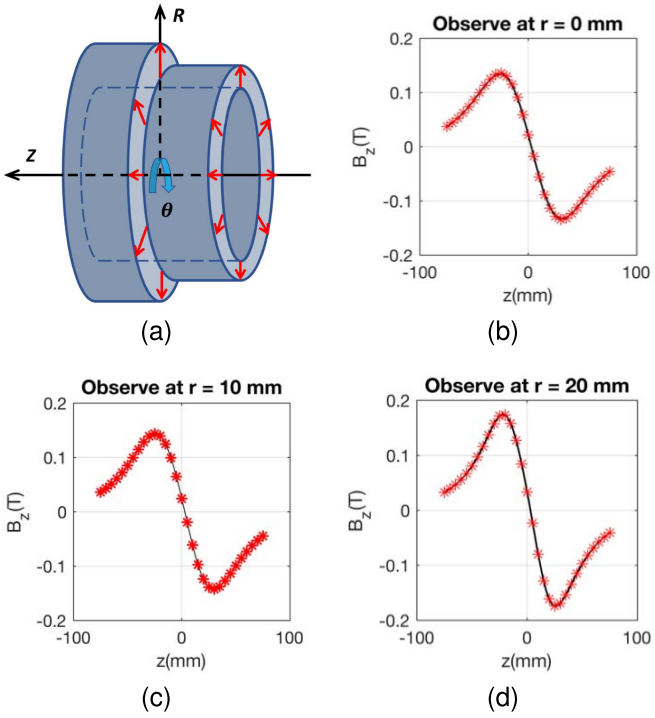

Fig. 5. (a) 3-D view of the magnet ring aggregate. Red arrows: polarization of two magnet rings. z-components of the magnetic field are calculated using both the current model (red stars) and COMSOL Multiphysics (black solid lines) on the cylindrical surfaces with (b) $r = 0$ mm, (c) $r = 10$ mm, and (d) $r = 20$ mm.

where M_0 is the magnitude of the remanent magnetization, z_1 and z_2 are the position of the front surface and the end surface of the ring along the z-axis, respectively. As shown in (2), the equivalent surface currents circulating on the front surface are clockwise whereas those on the end surface are anticlockwise. No surface currents are on the inner and outer side walls of the ring.

Since the magnet ring with continuously varying radial polarization is symmetric with respect to its radial axis, $\boldsymbol{B}(\boldsymbol{r})$ is θ independent, or in other words, axially symmetric. Therefore, only the fields on a specific θ need to be calculated for the fields in a 3-D space. The calculations on $\theta = 0$ were done, thus the observation point is defined as $\boldsymbol{r} = \langle r, 0, z \rangle$ and the derivation is simplified. The calculation is reduced to a 2-D problem. Substitute (2) into (1) with $\boldsymbol{r} = \langle r, 0, z \rangle$ and take the integration, (3) in the following is obtained:

$$\begin{aligned} &\boldsymbol{B}(\boldsymbol{r}) \\ &= \frac{\mu_0 M_0}{4\pi} \int_{R_{\text{in}}}^{R_{\text{out}}} \int_0^{2\pi} \\ &\quad \times \left(\frac{\langle r'(z_1 - z)\cos\theta', 0, rr'\cos\theta' - r'^2 \rangle}{[r^2 + r'^2 - 2rr'\cos\theta' + (z_1 - z)^2]^{3/2}} \right. \\ &\quad \left. - \frac{\langle r'(z_2 - z)\cos\theta', 0, rr'\cos\theta' - r'^2 \rangle}{[r^2 + r'^2 - 2rr'\cos\theta' + (z_2 - z)^2]^{3/2}} \right) d\theta' dr' \end{aligned} \tag{3}$$

where R_{in} and R_{out} are the inner and outer radius of the ring, respectively. As shown in (3), the θ-component of $\boldsymbol{B}(\boldsymbol{r})$ is zero. Equation (3) was applied to calculate the magnetic field

generated by a ring and ring aggregates. The calculated results are validated by comparing to the results using COMSOL Multiphysics, which is based on FEM. A two-ring aggregate as shown in Fig. 5(a) was calculated using both (3) and COMSOL Multiphysics. The two-ring aggregate consists of two magnet rings with the same inner radius of 40 mm, same thickness of 20 mm, and the outer radius of 60 and 50 mm, respectively. Both magnet rings are radially polarized outward. Fig. 5(b)–(d) shows the results calculated using (3) (in MATLAB) and those using COMSOL Multiphysics on different observation lines along the z-axis. As shown, the results using the simplified current model and COMSOL Multiphysics are in a good agreement with each other at different observation points. The time it takes for the calculation by applying (3) is only 1/10 of that by using COMSOL Multiphysics. With the validation, (3) with the principle of superposition is used for calculating the magnetic field generated by the magnet array in the optimization process. In the calculation, $\boldsymbol{B}$ field generated at $\boldsymbol{r} = \langle r, 0, z\rangle$ by a ring depends on the location and the dimension of the ring which is written as $\boldsymbol{B}(\boldsymbol{r}, R^i_{\text{in}}, R^i_{\text{out}}, z^i_1, z^i_2)$. Therefore, in the GA algorithm, the fields generated by the proposed ring-pair magnet array can be calculated using (4) as follows:

$$\boldsymbol{B}_{\boldsymbol{total}}(\boldsymbol{r}) = \sum_{j=1}^{2}\sum_{i=1}^{n}\left[\boldsymbol{B}\left(\boldsymbol{r}, R^i_{\text{in}}, R^i_{\text{out}}, z^{ij}_1, z^{ij}_2\right)\right] \tag{4}$$

where the superscript i indicates the ith ring pair with the first ring pair the outermost and the nth one the innermost (as shown in Fig. 2), n is the total number of ring pairs, and j indicates the ring on the left ($j = 1$) and that on the right ($j = 2$). In the proposed magnet array, the z-components of $\boldsymbol{B}_{\boldsymbol{total}}$ are used as the main magnetic field ($\boldsymbol{B_0}$) for MRI imaging. Therefore, an average $\boldsymbol{B_0}$ in the FOV can be calculated using the following equation:

$$\boldsymbol{B}_{0-\text{avg}} = \sum_{k=1}^{M} \boldsymbol{B}_z(\boldsymbol{r}_k)/M \tag{5}$$

where k is the index of the observation points in FOV and M is the total number of the points. In GA, a high $\boldsymbol{B_0}$ field strength is enforced by applying the constraint as follows:

$$\boldsymbol{B}_{0-\text{avg}} > 160 \text{ mT}. \tag{6}$$

The constraint is nonlinear because the relation of $\boldsymbol{B}_{0-\text{avg}}$ and the parameters being optimized is not linear. For the field homogeneity, the fitness function in ppm as defined as follows was applied:

$$\min\ f = \left\| \frac{\max_{1\le k\le M} \boldsymbol{B}_0(\boldsymbol{r}_k) - \min_{1\le k\le M} \boldsymbol{B}_0(\boldsymbol{r}_k)}{\boldsymbol{B}_{0-\text{avg}}} \right\| \times 10^6. \tag{7}$$

III. Results

The optimization was implemented in MATLAB multiple times, and it converged to a group of results that are not exactly the same. Among the results, a good candidate solution was selected based on not only the field homogeneity and field strength but also the geometry of the magnet array when the feasibility of the fabrication and assembly of an array was examined. The selected candidate solution is showed in Fig. 6. Fig. 6(a) shows that both the mean and the best fitness value (which indicate the field inhomogeneity) decrease as the number of iterations increases. The optimization stopped at the 335th iteration when the difference between two successive best individuals was within 10^{-12} for 50 iterations. Fig. 6(b) shows a 3-D view of the ring-pair magnet array with the best R^i_{in} which ranges between 150 and 220 mm. The optimized $[R^i_{\text{in}}](i = 1, 2, \ldots, 10)$ is [214 223 210 209 151 150 150 150 150 150] (unit: mm). As can be seen, the R^i_{in} determines the inner profile of the optimized magnet array. The optimized gap d is 200 mm.

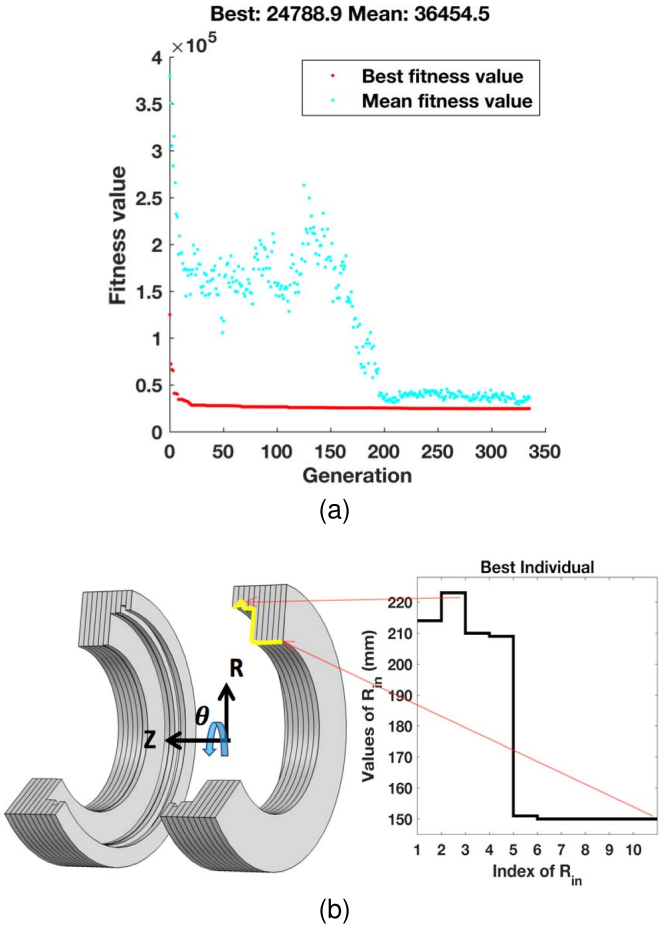

Fig. 6. (a) Change of fitness value versus iteration steps. (b) 3-D view of the optimized magnet array with the best $[R^i_{\text{in}}](i = 1, 2, \ldots, 10)$: [212 229 216 169 150 150 150 150 150 150] (unit: mm).

Fig. 7(a) and (b) plots the z-components of $\boldsymbol{B}$ ($\boldsymbol{B}_z$) generated by the optimized design in the plane when $z = 0$ (r–θ plane) and that when $\theta = 0$ (r–z plane), respectively, in the FOV calculated by (3) and (4). The $\boldsymbol{B}_z$ field is symmetric with respect to the z-axis, so the plot when $\theta = 0$ is symmetric to the plot when $\theta = \pi$ with respect to the z-axis. For a reference and comparison, an Aubert ring pair as shown in Fig. 1(d) was calculated. For a fair comparison, the outer radius and the thickness of the Aubert ring was set to be 250 and 100 mm, respectively, which are the same as the optimized proposed ring-pair array. The gap between

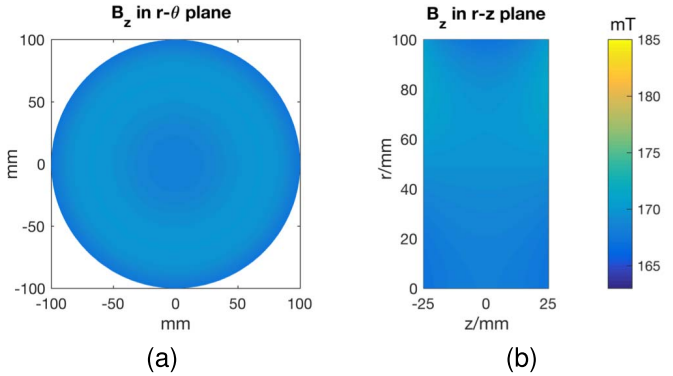

Fig. 7. Magnetic field generated by the optimized ring-pair design shown in Fig. 6(b) in FOV using the simplified current model in (a) r–θ plane and (b) r–z plane.

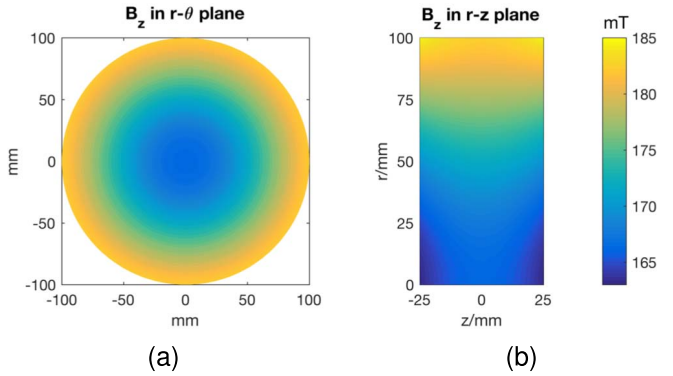

Fig. 8. Magnetic field generated by the reference Aubert ring pair shown in Fig. 1(d) in FOV using the simplified current model in (a) r–θ plane and (b) r–z plane.

the two Aubert rings was set to be 200 mm being the same as the gap of the innermost ring pair of the optimized array. Moreover, the inner radius of the Aubert ring pair was set to be 178.5 mm which guarantees the same amount of mass of magnetic materials of the two magnet arrays under comparison. Fig. 8(a) and (b) shows the plots of the calculated $\boldsymbol{B}_z$ generated by the reference Aubert ring pair in the $z = 0$ plane and that in the $\theta = 0$ plane, respectively, in the FOV. The calculation was done using (3) and (4).

Comparing the magnetic fields generated by the optimized array in Fig. 7 and those of an Aubert array with the same mass and similar dimensions in Fig. 8, in the same FOV, the optimized magnet array has a field homogeneity of 24 786 ppm and an average field strength of 169.7 mT whereas the reference magnet array has a field homogeneity of 122 150 ppm and an average field strength of 178.5 mT. As can be seen, the optimization reduces the inhomogeneity by over 79.7% with a sacrifice of the field strength of less than 5% (from 178.5 to 169.7 mT). The optimization offers significant improvement in field homogeneity while still maintains a similar field strength. The optimization results satisfy the preset optimization objective of an average field strength >160 mT and provide a field homogeneity of 24 786 ppm, which is very close to the objective of <20 000 ppm.

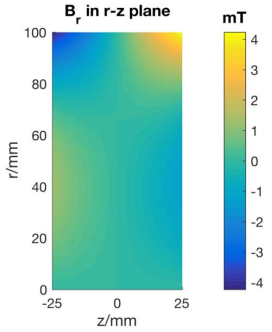

Fig. 9. r-components of the magnetic field generated by the optimized ring-pair design shown in Fig. 6(b) in FOV in the $\theta = 0$ plane using the simplified current model.

Fig. 9 shows the r-components of the optimized magnet array in the $\theta = 0$ plane. Comparing to the z-components as shown in Fig. 7(a), the r-components of the magnetic field generated by the proposed magnet array are much smaller than the z-components. The z-components dominate the field in the magnet array thus the field is in the longitudinal direction. When it is applied to supply $\boldsymbol{B}_0$ field for imaging, it is in the same relative orientation as that of a conventional superconducting magnet-based MRI scanner, which allows the application of available techniques for building RF coils to the system using the proposed magnet array. The optimized magnet array is suitable for providing the $\boldsymbol{B}_0$ field for a portable MRI system working with spatial encoding.

A magnet ring with a continuously varying radial polarization (inward or outward) is difficult to be fabricated. To facilitate an implementation, the proposed design is segmented into 12 identical fan-shaped magnets with a uniform polarization. The 3-D view of the magnet assembly is shown in Fig. 10(a). The segmented magnet assembly was simulated in COMSOL Multiphysics. The simulation results are shown in Fig. 10(b) and (c). The segmented magnet array has a field homogeneity of 32 511 ppm and an average field strength of 167.6 mT. Comparing to results of an array with continuously varying polarization in Fig. 7, owing to the discretization, the homogeneity of the field is reduced by 31.2% and the field strength is lowered by 1.24%. Comparing to the results of the ideal reference Aubert ring pair in Fig. 8, the inhomogeneity is still improved by 73.4%. Moreover, the reference Aubert ring pair was segmented and simulated using COMSOL Multiphysics. It shows a field homogeneity of 133 430 ppm and an average strength of 174.5 mT. Compared to the segmented reference Aubert ring, the segmented proposed design still shows an improvement of 75.6% in terms of the field inhomogeneity whereas a 4% reduction in terms of the average field strength. The results show that the discretization does not degrade the performance of the proposed magnet array much.

IV. Discussion

In this paper, the proposed design and optimization framework is flexible and effective. GA has a flexible definition of the fitness functions. Besides the field homogeneity and field strength, the optimization allows more design objectives that

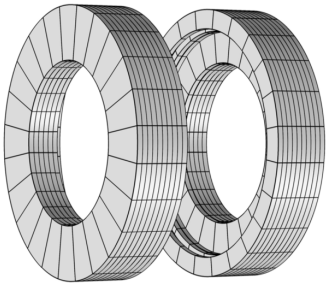

(a)

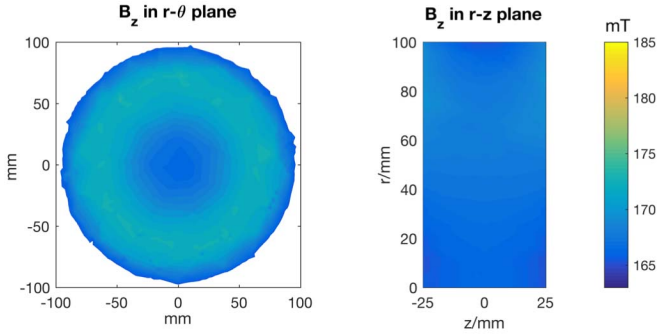

Fig. 10. (a) 3-D view of the segmented optimized magnet array made up of fan-shaped magnets is shown. The magnetic field generated by the segmented optimized magnet array in FOV simulated in COMSOL Multiphysics in (a) r–θ plane and (b) r–z plane.

are important to the design of a magnet array for a portable MRI, for example, lighter weight, more compact size, and a specific magnetic field pattern. Besides the application to a portable MRI system, the proposed design approach can be applied to design magnet arrays for other applications, such as accelerators and motors.

A specific $\boldsymbol{B}_0$ field pattern is needed for a portable MRI system to encode signals with information on the location where the need for gradient coils can be removed [2]. However, this field pattern should be generated within a certain field inhomogeneity, $\triangle \boldsymbol{B}_0$. The homogeneity corresponds to an RF bandwidth, $\Delta\omega$, which is expressed in the equation as follows:

$$\Delta\omega = \gamma\, \Delta \boldsymbol{B}_0 \tag{8}$$

where γ is the gyromagnetic magnetic ratio in MHz/T. In order to excite all the magnetic dipoles in the FOV, the bandwidth of an RF coil has to be greater or the same as $\Delta\omega$, $\Delta\omega_{\text{coil}} \geq \Delta\omega$. On the other hand, $\Delta\omega_{\text{coil}}$ has to be low to maintain high efficiency and a high Q-factor. Therefore, in the application of a magnet array for a portable MRI system where the magnetic field generated by the magnet array is used for encoding for imaging, $\boldsymbol{B}_0$ needs to have a certain amount of the inhomogeneity (with a pattern) for imaging but not too much to allow working with RF coils with a reasonable Q-factor. The FOV, in this paper, is a cylinder with a diameter of 200 mm and a length of 50 mm for 2-D head imaging. The length can be extended for 3-D imaging in the future.

In terms of the $\boldsymbol{B}_0$ field pattern, the proposed ring-pair magnet array provides a concentric-circled pattern as shown

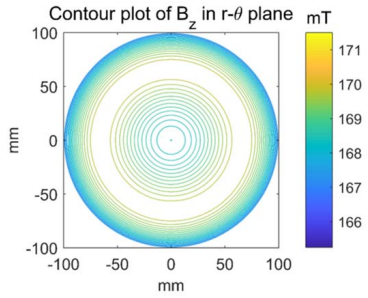

Fig. 11. Nonuniform concentric-circled pattern is shown.

in Fig. 11. This pattern can intrinsically spatially encode the signal in the r-direction, which is equivalently an always-on gradient field applied in the radial direction. For the application of this pattern for signal encoding for imaging, one method is to apply coil sensitivity encoding provided by rotating receiving coils to obtain additional information in the θ-direction for image reconstruction [24], [25]. Another possible solution is to introduce a rotating encoding magnetic block (or blocks) to break the radial symmetry of the magnetic field to bring additional information in the $\theta-$direction for image reconstruction [13]. The need for gradient coils can be removed in the aforementioned scenarios.

Compared with a Halbach magnet array, besides its compatibility to the existing RF coils, the proposed ring-pair design is easier to be fabricated and assembled to achieve a performance close to that of its counterpart with ideal magnetic polarization. The fan-shaped magnets (as proposed and shown in Fig. 10(a) are commonly used for electric motors, and they are commercially available. The housing structure for the proposed magnet array can be nylon rings with designed grooves that can be fabricated using standard fabrication procedure on computer numerical control machines, which is relatively easy compared to that for a sparse Halbach cylinder. The proposed design leads to a more compact size and a higher filling factor which is helpful to obtain a high field strength and a similar performance compared with the corresponding ideal design. A filling factor is defined as the ratio of the total mass of the magnet when an array is built to the mass of the magnet in the ideal model. The filling factor in Fig. 10(a) is almost 100%. However, for Halbach magnet array, the Halbach cylinders are often segmented into magnet bars, cylinders magnets [2], [11], [12], which leads to a relatively low filling factor. For the Halbach array in [11], the filling factor is only 32.5%. Although the sparse segmentation makes the structure lighter and less expensive, the field strength and homogeneity are considerably degraded. In terms of the fringe field of an array, the proposed design generates a stronger fringe field outside the magnet assembly compared to the Halbach array. One possible solution is covering the magnet assembly with high-permeability shields [15]. The high-permeability material could guide and concentrate the magnetic flux [26], thus greatly reduces the strength of the fringe field and strengthen the magnetic field inside.

Due to the inevitable imperfection of magnet materials and fabrication, there is non-negligible difference among the magnets in terms of remanent strength, and even the direction of

polarization. The effect of imperfect materials and fabrication should be identified and minimized. One way to minimize the effect of material imperfection is labeling, measuring, and sorting the magnets before assembling [14] thus those with serious defects could be discarded, and arrangement of magnets could be optimized. For magnet assembly, there are discrepancies between a defined location of a magnet and its real location. The accuracy of the position of the magnet can be increased if a housing is properly designed and fabricated with grooves of right dimensions for the magnets.

Another downside for permanent magnets is the slow degradation of remanence over time, also, they are temperature-sensitive. A relative thermostatic environment is needed, and the tracking of the field drift is necessary for the temperature compensation during the MRI scan. One possible solution to this problem is to add an NMR probe to the system to track the field strength drift caused by both temperature change and demagnetization effects [2].

V. Conclusion

We proposed the design and optimization of a ring-pair permanent magnet array for head imaging in a low-field portable MRI system. The proposed array generates a longitudinal $\boldsymbol{B}_0$ field with a magnetic field of 169.7 mT and a homogeneity of 24 786 ppm in an FOV with a diameter of 200 mm and a thickness of 50 mm. This is a reduction of 79.7% in terms of inhomogeneity yet a less than 5% reduction in field strength compared to a traditional ring-pair structure with a similar dimension and mass. The optimization was achieved by applying GA and proposing an efficient current model for the forward calculation. This efficient current model is a simplification of the traditional current model based on the unique arrangement of the magnets in the proposed design. The effectiveness of the optimization is validated by realistic simulations using COMSOL Multiphysics. With a longitudinal $\boldsymbol{B}_0$ field, the existing technology on RF coils for superconducting-magnet-based MRI scanners may directly be applied to an imaging system using the proposed magnet array. A more realistic 12-segmentation magnet assembly based on the optimized design is presented which shows a similar field strength and homogeneity with its non-segmented counterpart. It will be implemented in the near future for imaging.

Acknowledgment

This work was supported by Singapore-MIT Alliance for Research and Technology Innovation under Grant ING137068. Z. H. Ren would like to thank the support from the Singapore University of Technology and Design President Graduate Fellowship.

References

[1] T. Kimura *et al.*, "Development of a mobile magnetic resonance imaging system for outdoor tree measurements," *Rev. Sci. Instrum.*, vol. 82, no. 5, p. 053704, 2011.

[2] C. Z. Cooley *et al.*, "Two-dimensional imaging in a lightweight portable MRI scanner without gradient coils," *Magn. Reson. Med.*, vol. 73, no. 2, pp. 872–883, 2015.

[3] M. Sarracanie, C. D. LaPierre, N. Salameh, D. E. J. Waddington, T. Witzel, and M. S. Rosen, "Low-cost high-performance MRI," *Sci. Rep.*, vol. 5, Oct. 2015, Art. no. 15177.

[4] Z. H. Ren, S. Obruchkov, D. W. Lu, R. Dykstra, and S. Y. Huang, "A low-field portable magnetic resonance imaging system for head imaging," in *Proc. IEEE Progr. Electromagn. Res. Symp.-Fall (PIERS-FALL)*, Nov. 2017, pp. 3042–3044.

[5] P. S. Morgan, S. Conolly, and A. Mazovski, "Design of uniform field biplanar magnets," in *Proc. 5th Meeting ISMRM*, 1997, p. 1447.

[6] L. L. Tsai, R. W. Mair, M. S. Rosen, S. Patz, and R. L. Walsworth, "An open-access, very-low-field MRI system for posture-dependent 3He human lung imaging," *J. Magn. Reson.*, vol. 193, no. 2, pp. 274–285, 2008.

[7] H.-M. Klein, *Clinical Low Field Strength Magnetic Resonance Imaging: A Practical Guide to Accessible MRI*. Cham, Switzerland: Springer, 2015.

[8] *MAGNETOM C! 0.35T*. Accessed: Mar. 5. 2018. [Online]. Available: https://www.healthcare.siemens.com/magnetic-resonance-imaging/0-35-to-1-5t-mri-scanner/magnetom-c/technical-details

[9] K. Halbach, "Design of permanent multipole magnets with oriented rare Earth cobalt material," *Nucl. Instrum. Methods*, vol. 169, no. 1, pp. 1–10, 1980.

[10] G. Aubert, "Permanent magnet for nuclear magnetic resonance imaging equipment," U.S. Patent 5 332 971, Jul. 26, 1994.

[11] Z. H. Ren, L. Maréchal, W. Luo, J. Su, and S. Y. Huang, "Magnet array for a portable magnetic resonance imaging system," in *IEEE MTT-S Int. Microw. Symp. Dig.*, Sep. 2015, pp. 92–95.

[12] C. Z. Cooley *et al.*, "Design of sparse Halbach magnet arrays for portable MRI using a genetic algorithm," *IEEE Trans. Magn.*, vol. 54, no. 1, Jan. 2018, Art. no. 5100112.

[13] P. BlüMler, "Proposal for a permanent magnet system with a constant gradient mechanically adjustable in direction and strength," *Concepts Magn. Reson. B, Magn. Reson. Eng.*, vol. 46, no. 1, pp. 41–48, 2016.

[14] C. Hugon, P. M. Aguiar, G. Aubert, and D. Sakellariou, "Design, fabrication and evaluation of a low-cost homogeneous portable permanent magnet for NMR and MRI," *Comp. Rendus Chimie*, vol. 13, no. 4, pp. 388–393, 2010.

[15] K. Menzel, J. A. Lindner, H. Soltner, and H. Nirschl, "Design and application of a longitudinal field aubert permanent magnet composed of identically-shaped blocks for large-scale magnetic separation," *Separat. Purification Technol.*, vol. 134, pp. 220–231, Sep. 2014.

[16] K. Deb, A. Pratap, S. Agarwal, and T. Meyarivan, "A fast and elitist multiobjective genetic algorithm: NSGA-II," *IEEE Trans. Evol. Comput.*, vol. 6, no. 2, pp. 182–197, Apr. 2002.

[17] D. Whitley, "A genetic algorithm tutorial," *Statist. Comput.*, vol. 4, no. 2, pp. 65–85, Jun. 1994.

[18] N. R. Shaw and R. E. Ansorge, "Genetic algorithms for MRI magnet design," *IEEE Trans. Appl. Supercond.*, vol. 12, no. 1, pp. 733–736, Mar. 2002.

[19] Y. Yao, Y. Fang, C. S. Koh, and G. Ni, "A new design method for completely open architecture permanent magnet for MRI," *IEEE Trans. Magn.*, vol. 41, no. 5, pp. 1504–1507, May 2005.

[20] J. Chavanne, P. Elleaume, and O. Chubar, "Computing 3D magnetic fields from insertion devices," in *Proc. IEEE Particle Accelerator Conf.*, vol. 3, May 1997, pp. 3509–3511.

[21] O. Chubar, P. Elleaume, and J. Chavanne, "A three-dimensional magnetostatics computer code for insertion devices," *J. Synchrotron Radiat.*, vol. 5, no. 3, pp. 481–484, 1998.

[22] J.-S. Choi and J. Yoo, "Design of a Halbach magnet array based on optimization techniques," *IEEE Trans. Magn.*, vol. 44, no. 10, pp. 2361–2366, Oct. 2008.

[23] E. P. Furlani, *Permanent Magnet and Electromechanical Devices: Materials, Analysis, and Applications*. New York, NY, USA: Academic, 2001.

[24] K. P. Pruessmann *et al.*, "SENSE: Sensitivity encoding for fast MRI," *Magn. Reson. Med.*, vol. 42, no. 5, pp. 952–962, 1999.

[25] A. Trakic *et al.*, "Image reconstructions with the rotating RF coil," *J. Magn. Reson.*, vol. 201, no. 2, pp. 186–198, 2009.

[26] T. J. Sumner, J. M. Pendlebury, and K. F. Smith, "Convectional magnetic shielding," *J. Phys. D, Appl. Phys.*, vol. 20, no. 9, p. 1095, 1987.